Classification: PHYSICAL SCIENCES. Applied Physical Sciences

Title: Control of active liquid crystals with a magnetic field

Authors: Pau Guillamat, Jordi Ignés-Mullol, Francesc Sagués[*]

Affiliations:

Departament de Química Física, and Institute of Nanoscience and Nanotechnology (IN2UB), Universitat de Barcelona. Martí i Franquès 1, 08028 Barcelona. Catalonia. Spain.

*f.sagues@ub.edu

Abstract:

Living cells sense the mechanical features of their environment and adapt to it by actively remodeling their peripheral network of filamentary proteins, known as cortical cytoskeleton. By mimicking this principle, we demonstrate an effective control strategy for a microtubule-based active nematic in contact with a hydrophobic thermotropic liquid crystal. By employing well-established protocols for the orientation of liquid crystals with a uniform magnetic field, and through the mediation of anisotropic shear stresses, the active nematic reversibly self-assembles with aligned flows and textures that feature orientational order at the millimeter scale. The turbulent flow, characteristic of active nematics, is in this way regularized into a laminar flow with periodic velocity oscillations. Once patterned, the microtubule assembly reveals its intrinsic length and time scales, which we correlate with the activity of motor proteins, as predicted by existing theories of active nematics. The demonstrated commanding strategy should be compatible with other viable active biomaterials at interfaces, and we envision its use to probe the mechanics of the intracellular matrix.

Significance Statement:

Active liquid crystals are aqueous *in-vitro* suspensions of cytoskeletal proteins that self-assemble into elongated fibers, and develop sustained flows at the continuous expense of ATP. When they condense on soft interfaces, the aligned fibers organize into non-equilibrium analogues of passive liquid crystals. However, proteins do not respond to external electromagnetic fields, unlike liquid crystals, which are readily reconfigured inside devices. We demonstrate a reversible and biocompatible experimental protocol to align an active liquid crystal with a uniform magnetic field, allowing to transit between turbulent and laminar flow regimes. The active liquid crystal senses the interfacial viscous anisotropy

of a lamellar hydrophobic liquid crystal, not unlike the adaptation of cells to the mechanical features of their environment.

Main Text:

Liquid crystals are viscous fluids that self-assemble into equilibrium molecular arrangements featuring anisotropic physical properties that can be easily tailored by suitable boundary conditions, and reversibly rearranged by using modest electric or magnetic fields (*1*). These soft matter mesophases are not exclusive of artificial materials, as they are ubiquitous in lipid solutions (*2*), concentrated DNA fragments (*3*), and have been recently obtained by *in-vitro* cytoskeletal reconstitutions based on aqueous suspensions of filamentous proteins crosslinked by compatible molecular motors (*4-6*). The latter type of materials is referred to as active liquid crystals because, unlike their passive counterparts, they exhibit out-of-equilibrium behavior with supramolecular orientational order that is dynamically self-assembled at the continuous expense of hydrolizable adenosine triphosphate (ATP). Experiments with active soft matter (*7-17*) reveal new self-organizing features that are not present in passive materials. In spite of the vast richness of new behavior endowed by activity, traditional liquid crystals have a dramatic advantage: their orientation can be easily controlled to switch among different pre-designed configurations, which is crucial for the operation of devices, and for fundamental research in partially ordered materials. Contrarily, experiments on active nematics have relied on establishing their composition, confinement geometry, or activity as design parameters, but they lack true control capabilities of the resulting dynamic self-assembly. This limits their potential to serve as in-vitro model systems of the intracellular matrix or for the development of new functional biomaterials. Here, by interfacing an active nematic film with a hydrophobic oil that features smectic (lamellar) liquid-crystalline order (*18*), we reversibly align the originally turbulent flow of the active fluid into well-designed laminar flow directions by means of a magnetic field.

Results and discussion:

The chosen active material is an aqueous gel based on the self-assembly of micron-sized stabilized microtubules (*4, 19*). The latter are cross-linked and locally sheared by clusters of ATP-fueled kinesin motors, which are directed towards the plus ends of the microtubules. Thus, inter-filament sliding occurs in bundles containing microtubules of opposite polarity (Figure S1). This mixture arranges into an extensile active gel (*20-22*), continuously rebuilt following bundle reconstitution, and permanently permeated by streaming flows. An active nematic is obtained by concentrating this bulk material, using a depletion force, towards a

biocompatible soft and flat interface, usually a surfactant-decorated isotropic oil. Assembled filaments continuously fold and adopt textures typical of a two-dimensional nematic phase (*4*). This active film appears punctuated by a steady number of continuously renovated microtubule-void regions that configure semi-integer defect areas (Fig. 1A). In our case, the active nematic is formed at the interface between the aqueous protein suspension and a volume of the hydrophobic oil octyl-cyanobiphenyl (8CB), which features two liquid crystal phases at temperatures compatible with protein activity. The 8CB/water interface is stabilized with a polyethylene glycol (PEG)-based triblock copolymer surfactant, which also promotes the alignment of the thermotropic liquid crystal molecules parallel to the interface. Real time observation is performed using fluorescence, polarization, and confocal microscopies (see Experimental Methods).

When the thermotropic liquid crystal across the flat interface features the nematic phase (*T* > 33.4 °C), the active nematic displays the usual self-sustained turbulent flow characterized by the random proliferation of ±1/2 defects that unbind in pairs during spontaneous filament folding (*23-26*) (Fig. 1A). The dynamic viscosity of nematic 8CB is 30 mPa s (Fig. S2), which is significantly higher than that of isotropic oils earlier employed in the literature (*4*). This results in a lower average speed of the active flow, and a higher defect density for the same concentration of ATP, a clear evidence of the hydrodynamic influence that the passive fluid exerts on the active one. When our experiment is performed in the presence of a uniform in-plane magnetic field of 4 kG, created by a permanent magnet array (see Experimental Methods), 8CB molecules align with the field due to the positive diamagnetic anisotropy of this material. Nevertheless, we cannot detect any resulting alteration in the structure or in the dynamics of the active nematic underneath (Fig. 1B).

In order to increase the interfacial shear stress anisotropy, we quench the temperature below 33.4 °C, which results in 8CB transiting into the lamellar smectic-A (SmA) phase, which is characterized by molecules organized perpendicular to the lamellar planes. The active nematic rapidly rearranges due to the new boundary conditions (Fig. 1C,D and video S1), so that the chaotic filament orientation is now regularized into parallel stripes of uniform width aligned perpendicularly to the magnetic field. Fluorescence microscopy indicates that the bright stripes consist of densely packed microtubule bundles, while intercalated dark lanes incorporate the cores of proliferating ±1/2 defects, which align and move in antiparallel directions (Fig. 1D). During the slow temperature ramp, there is a transient state where regions with 8CB in the nematic and in the SmA phase coexist, resulting in growing areas where the active nematic is aligned, together with vanishing regions where it is still disordered (Fig. 1C). The active nematic adapts to the new interfacial state almost instantaneously for all explored activities (Video S2). The alignment process is reversible and versatile. By cycling the temperature above and below 33.4 °C (Fig. 1E-G) the active nematic returns to the disordered state when freed from the interfacial constraints (Fig. 1F),

and a new direction of alignment can be arbitrarily chosen by rotating the magnetic field (Fig. 1H and video S3).

This alignment effect can be understood by taking into account the structure of the contacting SmA phase. As mentioned above, 8CB molecules organize in planes perpendicular to their orientation, which is parallel to the magnetic field. Consequently, the SmA planes are perpendicular both to the 8CB/water interface and to the field (Fig. 1I). Polarizing optical microscopy confirms the formation of this aligned SmA layer (Fig. 1I), which includes dislocations in the aligned planes that propagate into the bulk forming the so-called parabolic focal conic domains (Fig. S3). It is well-known in the literature (*18*) that this *bookshelf* geometry of the SmA phase results in a liquid that flows easily when sheared along the planes, but responds as a solid to stresses exerted in the orthogonal direction. As a consequence of this configuration, the active nematic encounters an interfacial viscosity that is much higher for flow along the magnetic field than perpendicular to it, resulting in the observed alignment (Fig. 1 J,K).

The reported phenomenon is different from the alignment of a passive liquid crystal under shear flow. On the one hand, here the stress originates in the active fluid, and the interface provides only with a reconfigurable anisotropic template for alignment. On the other hand, there is no global net flow of the active nematic. As explained above, the aligned active filaments give rise to stripes intercalated by lanes with alternate antiparallel flow patterns (Fig. 1K). We have performed a velocimetry analysis on the moving active filaments (Fig. 2A,B) and have observed that the average speed is highest along the lanes where defect cores organize, and that it vanishes on the stripes where microtubules pack. Velocity gradients follow the complementary pattern, being the highest at the points of flow stagnation. By seeding the active nematic with tracer microparticles, we put into evidence that the aligned lanes are able to actively transport biocompatible cargo (Fig. 2C and video S4).

Recent models to describe the dynamic self-assembly of freely suspended active nematic films propose that steady-state patterns will be characterized by an intrinsic length scale, ℓ, which is the result of a balance between the forces required to deform the elongated microtubule bundles and the active stress provided by the molecular motors (*27*). This leads to a scaling relation $\ell^{-2} \sim \alpha$, where α is the activity parameter, linearly related to the chemical potential for ATP hydrolysis, $\alpha \sim \ln[\text{ATP}]$. We have analyzed the active nematic patterns aligned under a magnetic field for different activities, characterizing the spatial periodicity in terms of the average distance between adjacent antiparallel flow lanes. We find that this length scale depends on the ATP concentration as predicted by the above scaling relation (Fig. 3A, B), even though our active nematic film has a strong hydrodynamic coupling with the SmA 8CB, crucial to account for the described alignment

mechanism. Notice that the lane spacing in the aligned active nematic is completely uncorrelated to any characteristic length scale of the aligned SmA layer, such as the separation between dislocations of the smectic planes that can be observed in Fig. 1I. The SmA layer only sets an easy flow direction, while ℓ is an intrinsic property of the active nematic. Moreover, we find that the velocity inside lanes satisfies a scaling $v \sim \alpha$ (Fig. 3C). Existing theoretical models (*27*) predict this linear scaling in a laminar flow regime, while a dependence $v^2 \sim \alpha$ should be expected for active turbulence. In our case, the latter regime is observed when the active nematic is in contact with nematic 8CB or with an isotropic oil (Fig. S4). Therefore, we argue that the described alignment protocol provides with a reversible mechanism to transit the active nematic between the turbulent and the laminar flow regimes.

Parallel arrangement of microtubule bundles between defect lanes is prone to suffer the intrinsic bending instability of extensile active materials (*28, 29*). Indeed, we observe periodic bursts of defect creation across the stripes that lead to transient transversal flow (Fig. 2C). Regions with aligned stripes (denoted type I regions in Fig. 4A) coexist with transient regions where alignment is lost (denoted type II), which span arbitrary extensions that are commensurate with the stripe width. Close inspection shows that the instability originates from packed parallel microtubule bundles that bend and generate pairs of complementary half-integer defects, which either annihilate in pairs or incorporate into opposite lanes (Fig. 4B-D, video S5, and video S6).

We conjecture that these periodic events, which arise from the intrinsic dynamics of the sheared microtubules, provide a breakdown mechanism that the active material has at its disposition to repeatedly release the extensile tensional stress accumulated in the stripes (*30*). An analysis of the dynamics of the aligned active nematic layer reveals that these episodes occur with remarkable regularity. Slower defects are created in bursts, accompanied by a slowing down of the flow speed. This can be understood since transversal flow encounters a much higher interfacial viscosity conditions due to the anisotropy of the aligned SmA phase. Resulting velocity oscillations are characterized by a frequency that depends linearly on the activity (Fig. 4E-G). By considering that the rate of defect creation per unit area grows as α^2 (*27*), combined with the fundamental length scale defined above, we obtain an intrinsic time scale for the periodic rearrangement of the aligned material, τ, that satisfies the scaling relation $\tau^{-1} \sim \alpha$, consistent with our experimental observations (Fig. 4G). Recent numerical studies (*31*) have demonstrated that friction, rather than hydrodynamic coupling, can lead to the stabilization of active matter through defect ordering.

In conclusion, our work demonstrates that the disordered flow patterns of a two-dimensional active nematic can be controlled to follow preassigned directions by means of

a magnetic field, similarly to well-stablished strategies for the alignment of liquid crystals. The demonstrated technique, based on tailoring the anisotropy of the interface, overcomes the limitations of the protein-based active material in terms of directly addressing it with electric or magnetic fields. The described protocol enables to reversibly cycle through the different dynamic flow regimes of the kinesin/tubulin active nematic, including the usual active turbulent flow, and a newly observed laminar regime. The interface provides with a template for alignment that is versatile, in-situ reconfigurable, and compatible with viable active subcellular materials. Once the active nematic is aligned, intrinsic length and time scales are clearly evidenced, providing with an invaluable tool to contrast existing and future theoretical models that ultimately aim at understanding the dynamics of the active subcellular matrix, which is known to sense the mechanical properties of its environment (*32*).

Materials and Methods

Protein preparation. Microtubules (MTs) were polymerized from heterodimeric (α,β)-tubulin from bovine brain (a gift from Z. Dogic's group in Brandeis University), incubated at 37 ℃ for 30 min in aqueous M2B buffer (80 mM PIPES, 1 mM EGTA, 2 mM $MgCl_2$) prepared with Milli-Q water. The mixture was supplemented with the reducing agent dithiothrethiol (DTT, Sigma, 43815) and with Guanosine-5'-[(α,β)-methyleno]triphosphate (GMPCPP, Jena Biosciences, NU-405), a slowly hydrolysable analogue of the biological nucleotide Guanosine-5'-triphosphate (GTP) that completely suppresses the dynamic instability of the polymerized tubulin (*32*). GMPCPP enhances spontaneous nucleation of MTs (*33*) obtaining high-density suspensions of short MTs (1-2 μm). For fluorescence microscopy, 3% of the tubulin was labelled with Alexa-647. *Drosophila Melanogaster* heavy chain kinesin-1 K401-BCCP-6His (truncated at residue 401, fused to biotin carboxyl carrier protein (BCCP), and labelled with 6 Histidine tags) was expressed in *E.coli* using the plasmid WC2 from Gelles Lab (Brandeis University), and purified with a nickel column (*34*). After dialysis against 500 mM imidazole aqueous buffer, kinesin concentration was estimated by means of absorption spectroscopy. The protein was stored in a 60 % aqueous sucrose solution at -80 ℃ for future use (*33*).

Assembly of the MT-based active gel. Biotinylated kinesin motor protein and tetrameric streptavidin (Invitrogen, 43-4301) aqueous suspensions were incubated on ice for 30 minutes at the specific stoichiometric ratio 2:1 in order to obtain kinesin-streptavidin motor clusters. MTs were mixed with the motor clusters that acted as cross-linkers, and with ATP (Sigma, A2383) that drove the activity of the gel. The aqueous dispersion contained a non-adsorbing polymeric agent (polyethylene glycol, PEG, 20kDa, Sigma, 95172) that promoted the formation of filament bundles through depletion (Fig. S1). In order to maintain a constant concentration of ATP during the experiments, an enzymatic ATP-regenerator system was used, consisting on Phosphoenolpyruvate (PEP, Sigma, P7127) that fueled Pyruvate

kinase/lactate dehydrogenase (PK/LDH, Invitrogen, 434301) to convert ADP back into ATP. Several anti-oxidant components were also included in the solution in order to avoid protein denaturation, and to minimize photobleaching during characterization by means of fluorescence microscopy. The PEG-based triblock copolymer surfactant Pluronic F-127 (Sigma, P-2443) was added at 2 %w/w (final concentration) in order to procure a biocompatible water/oil interface in subsequent steps.

Active nematic cell. The active nematic/passive liquid crystal interface was prepared in a cylindrical pool of diameter 5 mm and depth 8 mm, manufactured with a block of Poly-dimethylsiloxane (PDMS) using a custom mold. The block was glued onto a bioinert and superhydrophilic polyacrylamide-coated glass (*35*) (see SI Text for additional details and a sketch of the setup). The pool was first filled with 50 μL of 4-cyano-4'-octylbiphenil (8CB, Synthon, ST01422; see SI Text for molecular structure and relevant physical properties of 8CB) and, subsequently, 1 μL of the water-based active gel was injected between the hydrophobic liquid crystal and the superhydrophilic glass plate. The polymeric surfactant at the water/8CB interface ensures a planar alignment of the mesogen molecules. Samples were placed inside a thermostatic oven built with Thorlabs SM1 tube components and tape heater, and controlled with a Thorlabs TC200 controller. The system was heated up to 36 °C in order to promote transition to the less viscous nematic phase of 8CB, which facilitated the spreading of the active gel onto the polyacrylamide-coated substrate. After several minutes at room temperature, the active material in the gel spontaneously condensed onto the flat water/8CB interface, leading to the formation of the active nematic layer. Unlike conventional flow cells, in which a layer of the active gel is confined in a thin gap between two glass plates, this setup enabled us to use high viscosity oils to prepare the interface. The thermostatized assembly was placed in the cavity of a cylindrical permanent magnet array that provided a uniform magnetic field of up to 4 kG parallel to the substrate (see SI Text for details on the magnet setup).

Sample characterization. Routine observations of the active nematic were performed by means of conventional epifluorescence microscopy. We used a custom-made inverted microscope with a halogen light source and a Cy5 filter set (Edmund Optics). Image acquisition was performed with a QImaging ExiBlue CCD cooled camera operated with ImageJ μ-Manager open-source software. For sharper imaging of the interfacial region, we employed laser-scanning confocal microscopy with a Leica TCS SP2 equipped with a photomultiplier as detector and a HeNe-633 nm Laser as light source. We performed confocal acquisition both in fluorescence and reflection modes. While fluorescence confocal microscopy optimizes the signal/noise ratio for improved imaging of the interfacial material, we found that reflection confocal microscopy was optimal for image velocimetry of the active nematic due to the enhanced acquisition rate. Moreover, the latter technique can be employed with label-free active nematic, thus significantly simplifying sample preparation, reducing material costs, and, more importantly, eliminating extraneous moieties that might alter the

way kinesin motors walk along the MTs. Tracer-free velocimetry analysis of the active nematic was performed with a public domain particle image velocimetry (PIV) program implemented as an ImageJ plugin (36). Further analysis of raw ImageJ output data was performed with custom-written MatLab codes. Particle flow velocimetry was performed by dispersing PEG-protected polystyrene microparticles of diameter 12 μm (PEGylated Polystyrene beads, Micromod, 08-56-124).

Figure Captions

Figure 1. Alignment of the active nematic with a magnetic field. (**A**) Fluorescence micrograph of the active nematic with a pair of complementary +1/2 (blue) and -1/2 (red) defects highlighted. (**B-H**) Fluorescence micrographs with different configurations of the active nematic in the presence of a 4kG uniform magnetic field. (**B**) The active fluid is initially in contact with nematic 8CB, which is transited, below $T_0 = 33.4$ °C, into the lamellar smectic-A phase (**C**) under a horizontal magnetic field. (**D**) The active nematic aligns perpendicularly to the field. By temperature cycling above (**E-F**) and below (**G-H**) T_0 under a vertical magnetic field, the active nematic is now realigned in the orthogonal direction (**H**). Pairs of aligned defects are highlighted in **D** and **H**. (**I**) Polarizing optical micrograph, and configuration of the underlying molecular planes in the SmA phase of the passive liquid crystal. (**J**) Fluorescence confocal micrograph revealing the correlation between the aligned active nematic and the anisotropic SmA phase. (**K**) Time average of the dynamic pattern. The arrows depict the antiparallel flow directions along the lanes of defect cores. Scale bars 100 μm.

Figure 2. Active flow along self-organized lanes. (**A**) Local velocity (vector plot) and local normalized vorticity ($\partial v_y/\partial x - \partial v_x/\partial y$, color density plot) in a vertically aligned active nematic film. A transversal cut of the time-averaged fluorescence micrograph is shown above the plot. (**B**) Downstream average of velocity and vorticity across the horizontal position. (**C**) Fluorescence micrograph with the path of colloidal tracers being advected in neighboring (i.e. antiparallel) flow lanes. Local instability of the aligned pattern may lead to lane jumps (middle panel) and thus to velocity inversion (bottom panel) of the transported particles. Scale bar 100 μm.

Figure 3. Activity dependence of the self-organized flows. (**A**) Time average of fluorescence micrographs of horizontally aligned active nematic films for different concentrations of ATP, from left to right 1400 μM, 700 μM, 470 μM, 280 μM, and 140 μM. Scale bar 100 μm. (**B**) Scaling of the average spacing between neighboring lanes, and (**C**) of the maximum speed inside the flowing lanes with the ATP chemical potential.

Figure 4. Oscillatory instability of the aligned active nematic. (**A**-**C**) Fluorescence micrographs of a horizontally-aligned active nematic layer showing the two alternating dynamic regimes, (I) with aligned stripes and lanes with flowing defects, and (II) with transversal flow. (**B**) Magnified view of regime (I) with the cores of the flowing +1/2 (blue circles) and -1/2 (red triangles) defects highlighted. (**C**) Magnified view of regime (II) with the proliferation of transversally flowing defect pairs. Scale bars 100 μm. (**D**) Instantaneous defect speed, and total number of defects in a region of size 190μm×190μm, for an ATP concentration of 140 μM, during spontaneous alternation between type I and type II regimes. (**E**) Temporal evolution of the average active nematic speed, determined from velocimetry measurements for different concentrations of ATP, 1400 μM (green), 700 μM (blue), 70 μM (red), and 35 μM (purple). (**F**) Normalized power spectra for data in (E). (**G**) Linear scaling of the leading oscillation frequency with the ATP chemical potential.
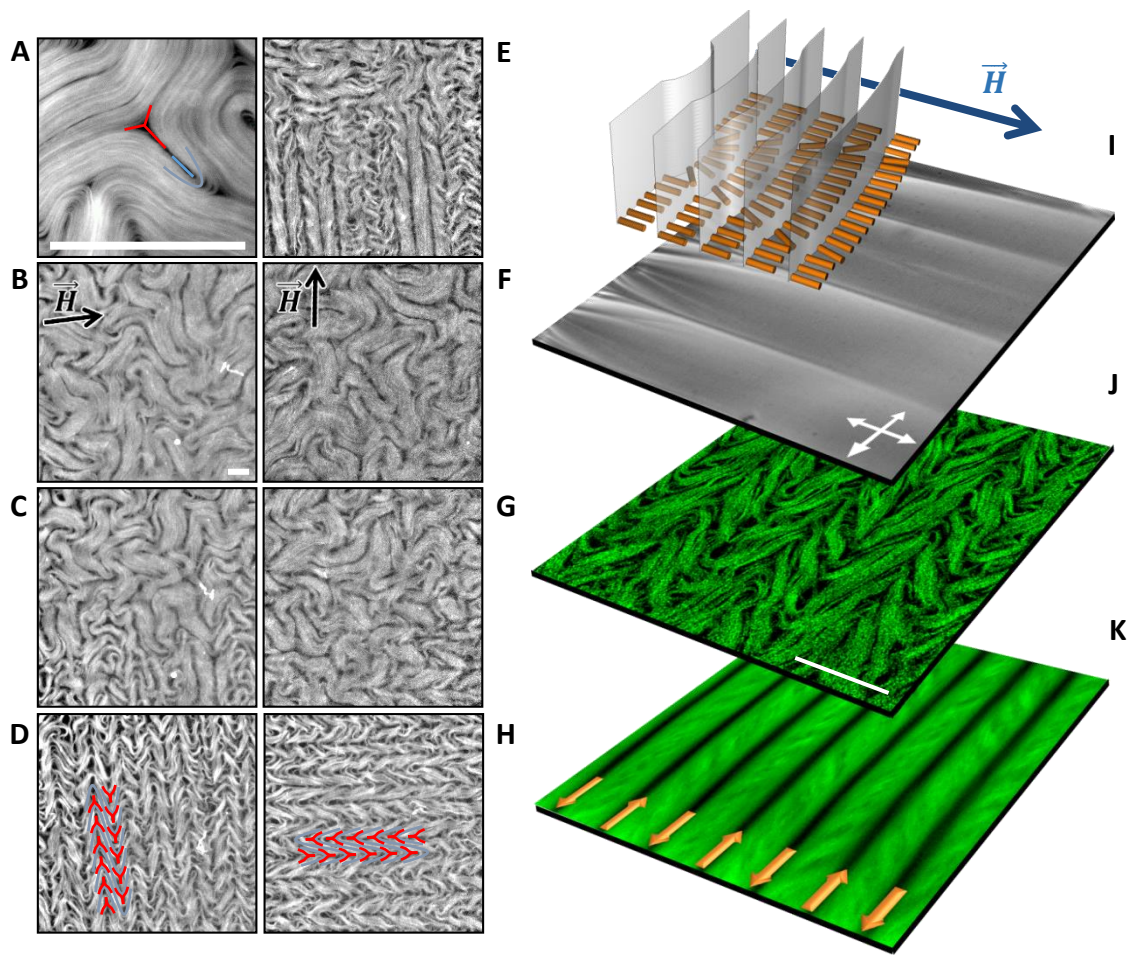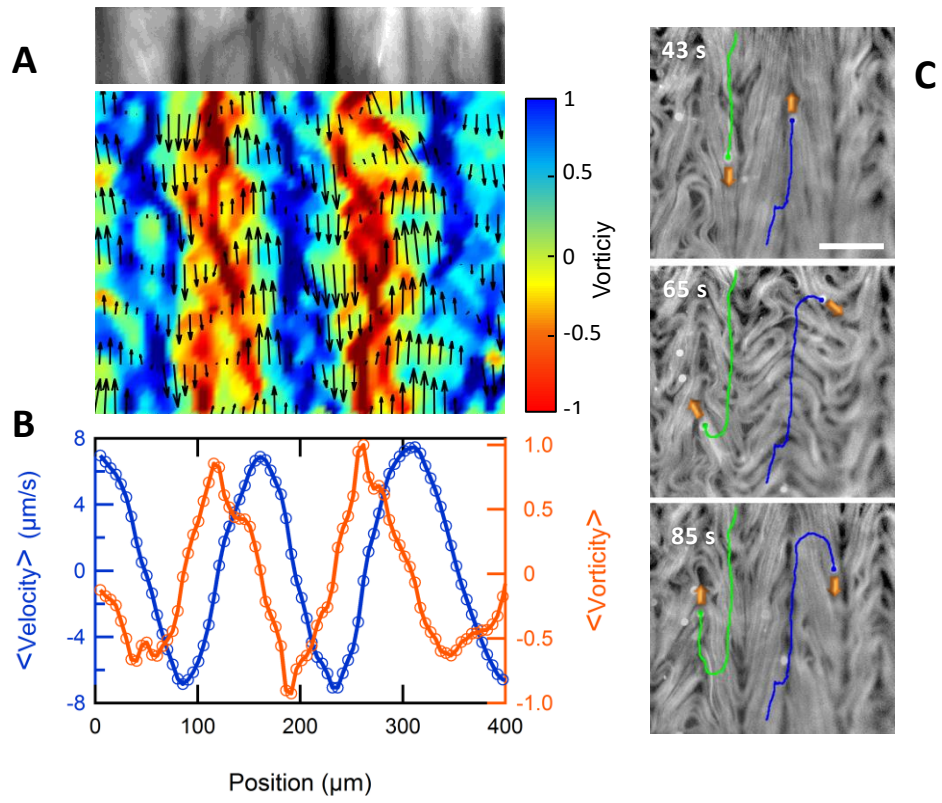
Figure 1.

A

B

C

43 s

65 s

85 s

<Velocity> (µm/s)

<Vorticity>

Position (µm)

Vorticiy

Figure 2.

A

B

4×10^{-4}

$<$ lane spacing $>^{-2} (\mu m^{-2})$

3

2

1

5   6   7

ln([ATP]/1.0μM)

C

speed (μm s^{-1})
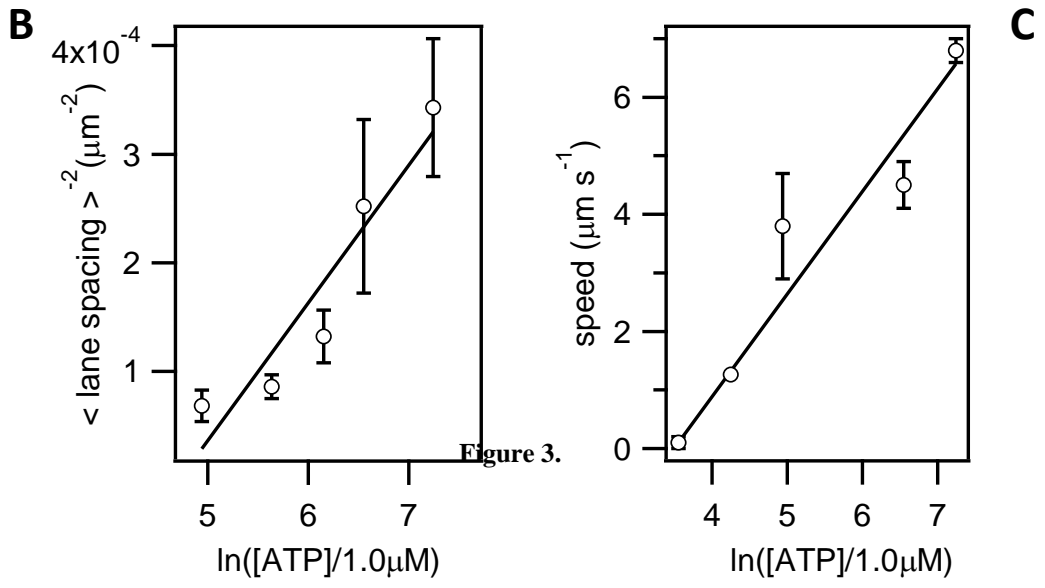
6

4

2

0

4   5   6   7

ln([ATP]/1.0μM)

Figure 3.

13
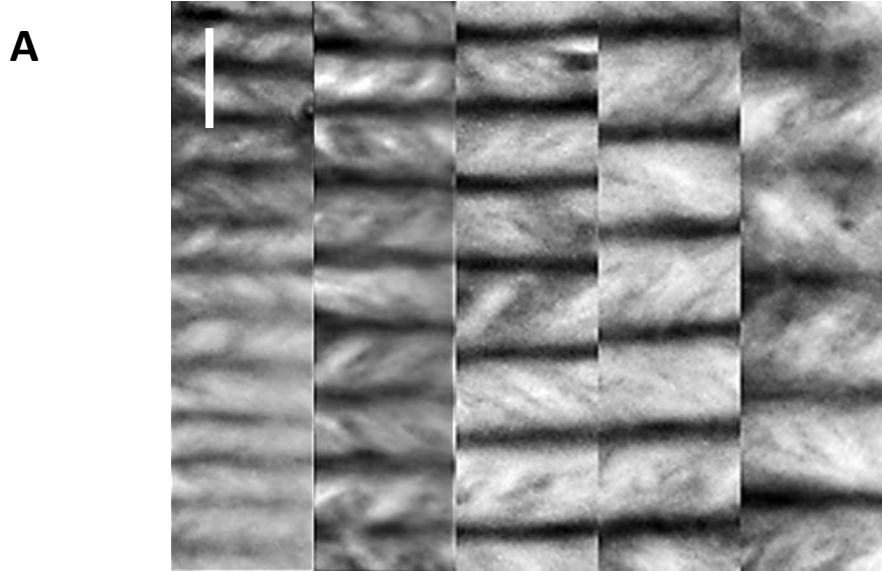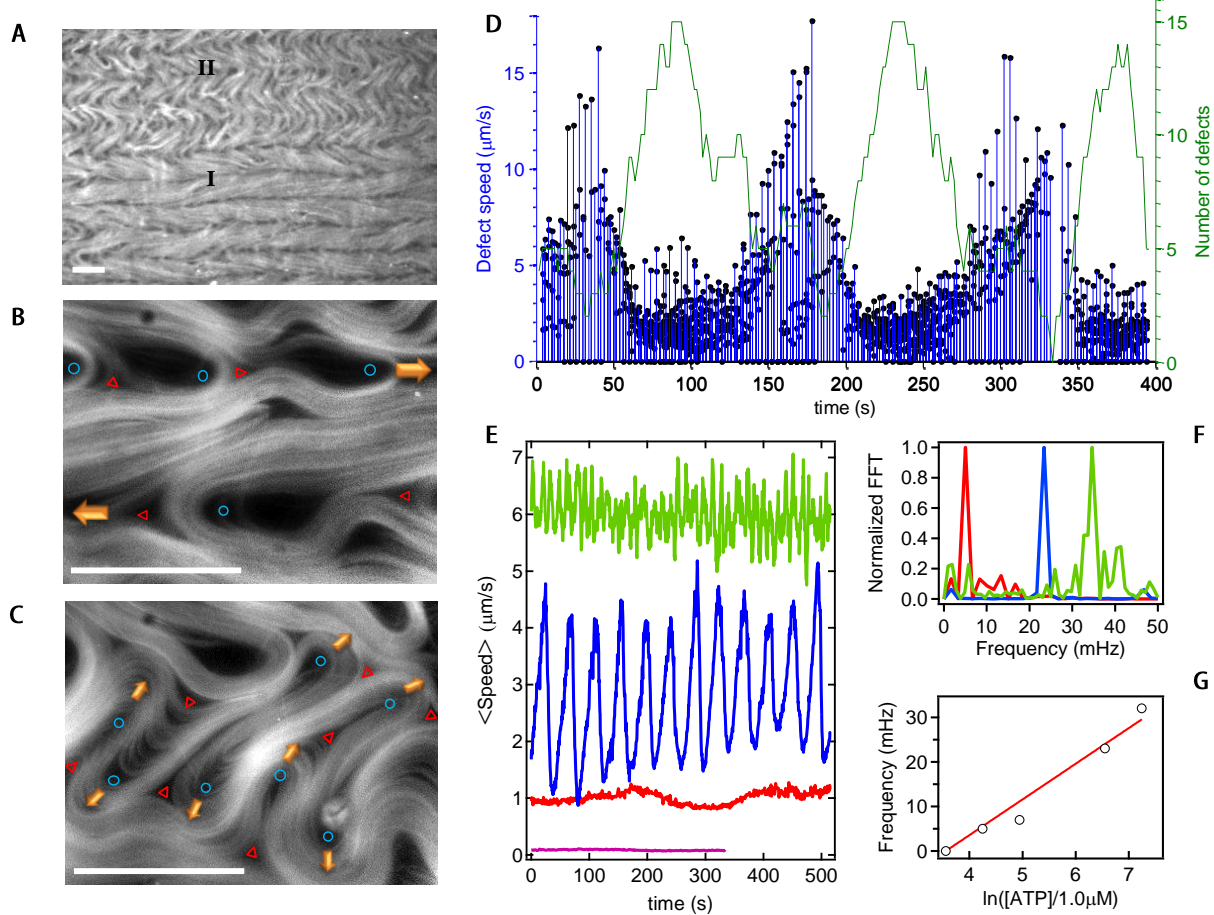
Figure 4.

References

1. P. Oswald, P. Pieranski, *Nematic and cholesteric liquid crystals : concepts and physical properties illustrated by experiments*. The liquid crystals book series (Taylor & Francis, Boca Raton, 2005).
2. I. W. Hamley, *Introduction to soft matter - revised edition : synthetic and biological self-assembling materials/ Ian W. Hamley*. (Wiley, Hoboken, N.J., Rev. ed., 2007).
3. T. E. Strzelecka, M. W. Davidson, R. L. Rill, Multiple liquid crystal phases of DNA at high concentrations. *Nature* **331**, 457 (1988).
4. T. Sanchez, D. T. Chen, S. J. DeCamp, M. Heymann, Z. Dogic, Spontaneous motion in hierarchically assembled active matter. *Nature* **491**, 431 (2012).
5. F. C. Keber *et al.*, Topology and dynamics of active nematic vesicles. *Science* **345**, 1135 (2014).
6. S. J. DeCamp, G. S. Redner, A. Baskaran, M. F. Hagan, Z. Dogic, Orientational order of motile defects in active nematics. *Nature materials* **14**, 1110 (2015).
7. T. Surrey, F. Nedelec, S. Leibler, E. Karsenti, Physical properties determining self-organization of motors and microtubules. *Science* **292**, 1167 (2001).
8. E. Karsenti, F. Nedelec, T. Surrey, Modelling microtubule patterns. *Nature cell biology* **8**, 1204 (2006).
9. V. Schaller, C. Weber, C. Semmrich, E. Frey, A. R. Bausch, Polar patterns of driven filaments. *Nature* **467**, 73 (2010).
10. S. Kohler, V. Schaller, A. R. Bausch, Structure formation in active networks. *Nature materials* **10**, 462 (2011).
11. V. Schaller, C. A. Weber, B. Hammerich, E. Frey, A. R. Bausch, Frozen steady states in active systems. *Proceedings of the National Academy of Sciences of the United States of America* **108**, 19183 (2011).
12. Y. Sumino *et al.*, Large-scale vortex lattice emerging from collectively moving microtubules. *Nature* **483**, 448 (2012).
13. V. Schaller, A. R. Bausch, Topological defects and density fluctuations in collectively moving systems. *Proceedings of the National Academy of Sciences* **110**, 4488 (2013).
14. S. Ramaswamy, The Mechanics and Statistics of Active Matter. *Annual Review of Condensed Matter Physics* **1**, 323 (2010).
15. M. C. Marchetti *et al.*, Hydrodynamics of soft active matter. *Reviews of Modern Physics* **85**, 1143 (2013).
16. T. Gao, R. Blackwell, M. A. Glaser, M. D. Betterton, M. J. Shelley, Multiscale polar theory of microtubule and motor-protein assemblies. *Physical review letters* **114**, 048101 (2015).
17. S. Zhou, A. Sokolov, O. D. Lavrentovich, I. S. Aranson, Living liquid crystals. *Proceedings of the National Academy of Sciences of the United States of America* **111**, 1265 (2014).
18. P. Oswald, P. Pieranski, *Smectic and columnar liquid crystals : concepts and physical properties illustrated by experiments*. The liquid crystal book series (Taylor & Francis, Boca Raton, FL, 2006).
19. G. Henkin, S. J. DeCamp, D. T. Chen, T. Sanchez, Z. Dogic, Tunable dynamics of microtubule-based active isotropic gels. *Philosophical transactions. Series A* **372**, (2014).
20. F. Julicher, K. Kruse, J. Prost, J. Joanny, Active behavior of the Cytoskeleton. *Physics Reports* **449**, 3 (2007).
21. K. Kruse, J. F. Joanny, F. Julicher, J. Prost, K. Sekimoto, Generic theory of active polar gels: a paradigm for cytoskeletal dynamics. *The European physical journal. E* **16**, 5 (2005).
22. J. Prost, F. Jülicher, J. F. Joanny, Active gel physics. *Nature Physics* **11**, 111 (2015).
23. L. Giomi, M. J. Bowick, X. Ma, M. C. Marchetti, Defect annihilation and proliferation in active nematics. *Physical review letters* **110**, 228101 (2013).
24. X. Q. Shi, Y. Q. Ma, Topological structure dynamics revealing collective evolution in active nematics. *Nature communications* **4**, 3013 (2013).
25. S. P. Thampi, R. Golestanian, J. M. Yeomans, Velocity correlations in an active nematic. *Physical review letters* **111**, 118101 (2013).
26. C. A. Weber, C. Bock, E. Frey, Defect-mediated phase transitions in active soft matter. *Physical review letters* **112**, 168301 (2014).

27. L. Giomi, Geometry and Topology of Turbulence in Active Nematics. *Physical Review X* **5**, 031003 (2015).

28. R. Aditi Simha, S. Ramaswamy, Hydrodynamic fluctuations and instabilities in ordered suspensions of self-propelled particles. *Physical review letters* **89**, 058101 (2002).

29. R. Voituriez, J. F. Joanny, J. Prost, Spontaneous flow transition in active polar gels. *Europhysics Letters* **70**, 404 (2005).

30. L. Giomi, L. Mahadevan, B. Chakraborty, M. F. Hagan, Excitable patterns in active nematics. *Physical review letters* **106**, 218101 (2011).

31. A. Doostmohammadi, M. F. Adamer, S. P. Thampi, J. M. Yeomans. Stabilization of active matter by flow-vortex lattices and defect ordering. *Nature communications* **7**, 10557 (2016).

32. M. Gupta *et al.*, Adaptive rheology and ordering of cell cytoskeleton govern matrix rigidity sensing. *Nature communications* **6**, 7525 (2015).

33. A. A. Hyman, S. Salser, D. N. Drechsel, N. Unwin, T. J. Mitchison, Role of GTP hydrolysis in microtubule dynamics: information from a slowly hydrolyzable analogue, GMPCPP. *Molecular Biology of the Cell* **3**, 1155 (1992).

34. R. Subramanian, J. Gelles, Two distinct modes of processive kinesin movement in mixtures of ATP and AMP-PNP. *The Journal of general physiology* **130**, 445 (2007).

35. A. W. C. Lau, A. Prasad, Z. Dogic, Condensation of isolated semi-flexible filaments driven by depletion interactions. *Europhysics Letters* **87**, 48006 (2009).

36. Q. Tseng *et al.*, Spatial organization of the extracellular matrix regulates cell-cell junction positioning. *Proceedings of the National Academy of Sciences of the United States of America* **109**, 1506 (2012).